

Modeling the BAO feature in Bispectrum

Jayashree Behera^{1*}, Mehdi Rezaie¹, Lado Samushia^{1,2,3}, and Julia Ereza⁴

¹*Department of Physics, Kansas State University, 116 Cardwell Hall, Manhattan, KS, 66506, USA*

²*E.Kharadze Georgian National Astrophysical Observatory, 47/57 Kostava St., Tbilisi 0179, Georgia*

³*School of Natural Sciences and Medicine, Ilia State University, 3/5 Cholokashvili Ave., Tbilisi 0162, Georgia*

⁴*Instituto de Astrofísica de Andalucía (CSIC), Glorieta de la Astronomía, E-18080 Granada, Spain*

7 June 2024

ABSTRACT

We investigate how well a simple leading order perturbation theory model of the bispectrum can fit the BAO feature in the measured bispectrum monopole of galaxies. Previous works showed that perturbative models of the galaxy bispectrum start failing at the wavenumbers of $k \sim 0.1h \text{ Mpc}^{-1}$. We show that when the BAO feature in the bispectrum is separated it can be successfully modeled up to much higher wavenumbers. We validate our modeling on GLAM simulations that were run with and without the BAO feature in the initial conditions. We also quantify the amount of systematic error due to BAO template being offset from the true cosmology. We find that the systematic errors do not exceed 0.3 per cent for reasonable deviations of up to 3 per cent from the true value of the sound horizon.

Key words: galaxies: statistics - cosmological parameters - large-scale structure of Universe

1 INTRODUCTION

The Baryon Acoustic Oscillation (BAO) signal is a statistical feature imprinted into the spatial distribution of galaxies. Small overdensities in the initial distribution of dark matter serve as seeds for acoustic wave propagation in the early baryon-photon fluid. The propagation of these waves freezes at later times and results in a slightly overdense spherical shell of a radius of about $r_d \sim 100h^{-1} \text{ Mpc}$ around each primordial overdensity. From the observational point of view, this means that every galaxy created around the initial overdensity has a slightly higher chance of having a neighboring galaxy on this spherical shell. Later this feature manifests itself as a local maximum (peak) at r_d in the two-point correlation function of galaxies and as a decaying oscillatory feature of frequency $2\pi/r_d$ in the power spectrum. The BAO scale has been measured from the two-point correlation function with a sub-percent precision. Theoretical modeling and interpretation of the measured BAO scale in the two-point correlation function are relatively straightforward. The measurements in conjunction with the theory can be used to determine the distance-redshift relationship and therefore to constrain cosmological models. The same feature must also be present in other measures of galaxy clustering but it may not be as easy to model. The main goal of our paper is to explore the possibility of modeling the BAO feature in the Fourier space measurements of the galaxy three-point correlation function.

Many methods for measuring the BAO peak position (or frequency) have been proposed in recent years. They all follow the same schematic idea proposed in Eisenstein et al. (2007).

- Theoretically computed two-point correlation function (or the power spectrum) is split into “smooth” and “wiggly” components,

* E-mail: jayashreeb@phys.ksu.edu

$\xi = \xi_s \xi_w$ or $P = P_s P_w$. This can be done in many different ways but the final result is not sensitive to details of the decomposition. With proper decomposition, P_w ends up being a decaying oscillation around unity (Baldauf et al. 2015; Vlah et al. 2015; Fonseca de la Bella et al. 2017).

- The wiggly component is separated from the measurements in a similar way.
- The leading order effect of non-linear evolution on the wiggly part of the power spectrum is scale-dependent damping of the oscillations, $P_w \rightarrow (P_w - 1)D(k) + 1$. The simplest model $D(k) = \exp(-\Sigma^2 k^2)$, where Σ is a nuisance parameter, works reasonably well (Nomura et al. 2008; Crocce et al. 2012; Prada et al. 2016; Seo et al. 2016; Hoffmann et al. 2018; Chen et al. 2019; Hinton et al. 2020; Valageas & Nishimichi 2020; Sugiyama et al. 2021; Babić et al. 2022).
- The damped model is supplemented by nuisance parameters to account for small inaccuracies in separating the smooth part. These nuisance parameters are usually polynomials in k and they are smooth in the sense that they have little effect on the frequency of the oscillatory signal (Ross et al. 2017; Ata et al. 2018; Hou et al. 2021; Raichoor et al. 2021).
- The model is then dilated $P_w \rightarrow AP_w(\alpha k)$ to align its oscillations with the ones in the measurements.

In the simplest version of this analysis (when the fit is performed on the angularly averaged power spectrum), the dilation parameter α depends on the distance redshift relationship,

$$\alpha \equiv \alpha_V = \frac{D_V(z)r_d^{\text{tmp}}}{D_V^{\text{fid}}(z)r_d}, \quad (1)$$

where D_v is the distance to the galaxies,

$$D_v(z) = \left[\frac{czD_A(z)^2}{H(z)} \right]^{\frac{1}{3}}, \quad (2)$$

D_A is the angular diameter distance, and H is the Hubble parameter. The superscript fid denotes values in “fiducial” cosmology assumed when converting redshifts of galaxies to distances and the superscript tmp is used to denote the BAO scale in the BAO template which may be (but does not have to be) identical to the fiducial cosmology. Quantities without superscripts are the real values corresponding to the data. The fiducial values assumed in the theoretical model and the BAO peak position in the template are known exactly. Thus, measuring α allows us to infer the ratio of the distance at a given redshift to the BAO scale, a quantity that is extremely sensitive to the properties of dark energy. The exact procedure used in high-precision data analysis is more involved and requires great care in every small detail. The fit is performed to both the angular monopole and the quadrupole of the correlation function, which enables us to also measure the anisotropic dilation parameter $\epsilon = H^{\text{fid}} r_d^{\text{tmp}} / (H r_d)$ (Padmanabhan & White 2008; Reid et al. 2012; Blazek et al. 2014; Ross et al. 2015; Beutler et al. 2017b; Zhu et al. 2018; Hou et al. 2018, 2021), but the general idea remains the same. These scalings have been shown to be robust for a wide variety of cosmological models (Vargas Magaña et al. 2013; Thepsuriya & Lewis 2015; Ding et al. 2018; Vargas-Magaña et al. 2014).

This procedure for extracting the BAO signal from the power spectrum has been successfully used on many galaxy samples (Neveux et al. 2020; Bautista et al. 2021; de Mattia et al. 2021; Gil-Marín et al. 2020; Raichoor et al. 2021). The resulting distance measurements are leading sources of dark energy parameter constraints (Betoule et al. 2014; Aubourg et al. 2015; Alam et al. 2017; Grieb et al. 2017; Sánchez et al. 2017; Abbott et al. 2018; Alestas et al. 2020; d’Amico et al. 2020; Di Valentino et al. 2020; Ivanov et al. 2020; Planck Collaboration et al. 2020; Tröster et al. 2020; Escamilla et al. 2023).

The physics governing the production of Baryon Acoustic Oscillations (BAOs) in the matter power spectrum is well understood (Silk 1968; Peebles & Yu 1970; Sunyaev & Zeldovich 1970; Bond & Efstathiou 1984, 1987; Holtzman 1989). In the very early universe, the matter distribution was highly uniform. Small overdensities in this uniform distribution were growing in time with gravity, forming dark matter halos and later galaxies. Pulling matter into overdensities raised the temperature of matter, thereby creating an outward radiation pressure that pushed the matter apart again. As it expanded though, it cooled and gravity started to pull it back again. This interactivity between gravity and pressure set up an oscillation that created the equivalent of spherical sound waves that spread outward like bubbles. When the Universe reached the age of around 380,000 years, atoms formed for the first time. This allowed the matter to cool more efficiently, and gravity started to dominate over pressure. With no resistance from pressure, large-scale structures started to form. The wrinkles due to the bubbles of matter created by those acoustic waves are visible today as the baryon acoustic oscillations. The size of the oscillations is determined by the properties of the early Universe and its components: the baryonic matter, the dark matter, and the dark energy. Thus, they can be used to constrain the properties of these components. The imprint of the BAO is left in overdensity peaks at $r_d \sim 100$ Mpc in the two-point statistics of the matter field. Basically, these oscillatory features occur on relatively large scales, which are still predominantly in the linear regime; it is therefore expected that BAOs should also be seen in the galaxy

distribution (Meiksin et al. 1999; Springel et al. 2005; White 2005; Seo & Eisenstein 2005; Eisenstein et al. 2007).

The same BAO feature is also present in other clustering measures e.g. the three-point correlation function, or its Fourier image, the bispectrum. In general, the bispectrum is more difficult to model compared to the power spectrum. Recent studies showed that the perturbation theory based models fail to accurately predict bispectrum measurements at surprisingly large scales (Lazanu et al. 2016; Baldauf et al. 2021; Ivanov et al. 2022; Philcox et al. 2022; Alkhanishvili et al. 2022; Rizzo et al. 2023; Karandikar et al. 2023; Guidi et al. 2023). Several recent works managed to measure the distance scale from the BAO feature in the bispectrum despite these difficulties (Pearson & Samushia 2018; Philcox & Ivanov 2022). A number of recent works (Slepian & Eisenstein 2015; Slepian et al. 2017; Pearson & Samushia 2018) measured the BAO peak also in the galaxy three-point statistics. More works have studied different aspects of modeling the full bispectrum (Byun et al. 2015, 2017; Gil-Marín et al. 2017, 2018; Gualdi et al. 2019; Philcox & Ivanov 2022; Sugiyama et al. 2019, 2020, 2021, 2023a,b) and by comparing theoretical models of increasing difficulty with simulations (Oddo et al. 2020; Colavincenzo et al. 2019; Bose & Taruya 2018).

When it comes to the BAO peak position, studies tend to focus on two-point statistics (Anderson et al. 2012, 2014; Cuesta et al. 2016; Gil-Marín et al. 2016; Ross et al. 2017; Beutler et al. 2017a). This is justified by the fact that the reconstruction of the galaxy field (Eisenstein et al. 2007; Noh et al. 2009) moves some of the information from the three-point statistics – e.g. the three-point correlation function or the bispectrum – into the two-point statistics. However, measuring the BAO peak position from the bispectrum directly – or the combination of the non-reconstructed power spectrum and bispectrum – is still useful as the effect of the reconstruction on the information content of the higher-order statistics is, at the moment, not completely clear (Samushia et al. 2021).

In this work, we explore the possibility of isolating the BAO feature in the galaxy bispectrum and modeling it with a simple model supplemented by enough nuisance parameters to account for inaccuracies in modeling its overall shape. The BAO feature in the Fourier space extends to high wavenumbers, but the quantity of interest is not the exact profile of the feature as a function of a wavenumber but its frequency, which is set by large-scale physics. The hope is that, if the BAO feature in the bispectrum is isolated, it will be possible to model it effectively even if the modeling of the full bispectrum is difficult. Our results are encouraging and suggest that surprisingly simple models of the BAO feature in the bispectrum are able to reproduce the BAO frequency with minimal bias. This is not surprising as the BAO signal is imprinted by linear physics in the early Universe. While the exact amount of power at high wavenumbers is difficult to theoretically compute, the quantity of interest in the BAO analysis is the beat frequency of the feature, and this quantity turns out to be more robust.

We use a simple, linear-theory-based model to describe the BAO feature in the bispectrum, in which the effect of nonlinear evolution is modeled by a wavenumber-dependent Gaussian damping term. (see section 3). We use GLAM simulations (see section 2) to validate this model. These simulations were run in pairs with and without the BAO feature in the initial conditions but otherwise identical. These simulations provide us with the “empirical” data for the smooth and wiggly bispectra. When fitting our model to simulations, we find that the extracted BAO scale is unbiased even when the fiducial template for the BAO is constructed in a slightly offset cosmological model (see section 4). The recovered values of α are within 0.3 per cent

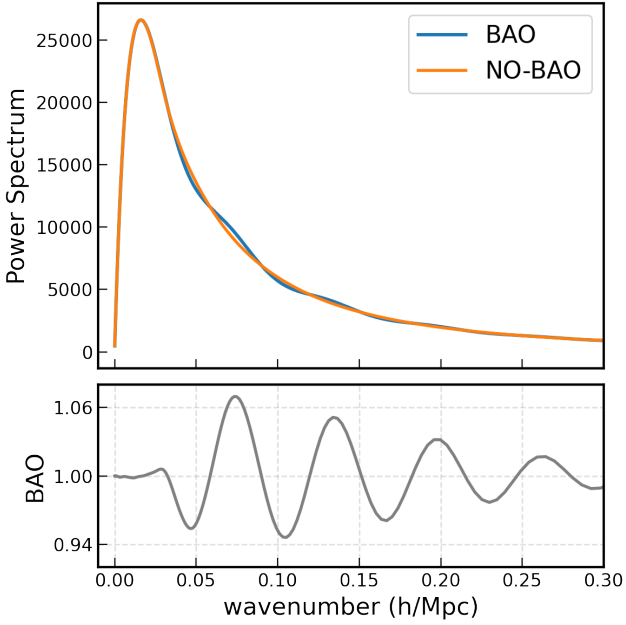


Figure 1. Initial power spectrum of GLAM *withBAO* and *noBAO* simulations and its BAO signature.

of the true values even when the BAO feature in the fitting template deviates from the true value by as much as 3 per cent.

2 BAO SIGNAL IN SIMULATIONS

2.1 GLAM simulations

We use GLAM-PMILL simulations (Hernández-Aguayo et al. 2021) to test methods for BAO feature separation and theoretical modeling. The GLAM-PMILL catalogs used in this work are publicly available in the SKIES & UNIVERSES website¹.

The GLAM simulations (Klypin & Prada 2018) are N -body cosmological simulations that, in the case of the PMILL series, follow the evolution of $2,000^3$ dark matter particles. Each particle has a mass of $1.065 \times 10^{10} h^{-1} M_{\odot}$ in a comoving periodic box of size $L = 1 h^{-1} \text{Gpc}$, with $N_s = 136$ time-steps and a mesh of $N_g = 4,000$ cells per side. This results in a spatial resolution of $0.250 h^{-1} \text{Mpc}$.

The simulations were produced in a flat ΛCDM cosmology, adopting the cosmological parameters assumed in the Planck Millennium simulation (PMILL; Baugh et al. 2019). PMILL uses the best-fitting parameters from the first Planck 2013 data release (Planck Collaboration et al. 2014). Each instance of the simulation was run with two initial conditions, starting at $z_{\text{ini}} = 100$: one with the BAO signal imprinted in the initial conditions, and one without. The pairs of simulations are otherwise identical, i.e. they had matching random phases in the initial conditions. The GLAM-PMILL simulations used in this work consist of 1,000 realizations with and another 1,000 without BAO. Figure 1 shows the power spectrum used for the initial conditions of the GLAM simulations. The initial power for the pair of simulations was identical, except the “withBAO” instances had

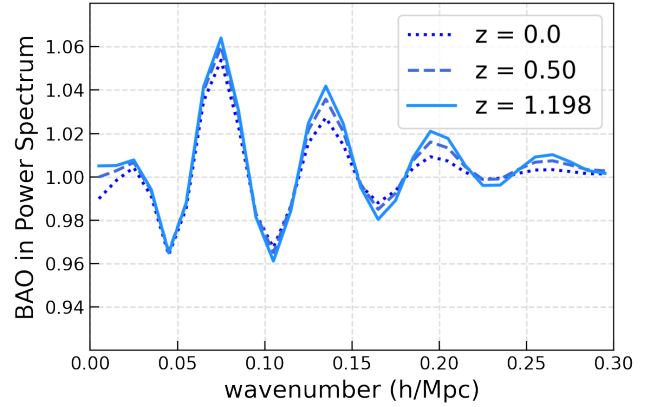


Figure 2. BAO signature in the power spectrum of GLAM simulations at different redshifts.

periodic BAO wiggles in them, and the “noBAO” instances didn’t have the feature.

The GLAM simulations are only capable of correctly resolving distinct halos (not subhalos), with virial masses greater than $\sim 10^{12} h^{-1} M_{\odot}$ for the case of the GLAM-PMILL suite. The resulting dark matter halos were populated by galaxies using GALFORM semi-analytical model of galaxy formation (Hernández-Aguayo et al. 2021), but in this work we only use the halo catalogs, both for BAO and noBAO realizations.

We will treat the measurements from these simulations as the ground truth for the rest of our work. The theoretical models will be evaluated based on how well they recover the measurements of GLAM simulations.

2.2 BAO in the power spectrum

We measure the power spectrum from both the *withBAO* and *noBAO* simulations, P_w and P_s respectively (see Appendix A for the details). The power spectrum measurements are averaged in bins of width $\Delta k = 0.01 h \text{Mpc}^{-1}$ starting from $k_{\text{min}} = 0.005 h \text{Mpc}^{-1}$ up to $k_{\text{max}} = 0.3 h \text{Mpc}^{-1}$, resulting in 30 bins. This wavenumber range contains most of the linear and semi-linear modes of galaxy overdensity. There is very little BAO signal above our maximum wavenumber.

Figure 2 shows the ratio of P_w to P_s measured from GLAM at different redshifts. This is by definition the BAO signal in the power spectrum. The BAO signal looks exactly as expected. The amplitude of wiggles decays with redshift. The decay is wavenumber-dependent. BAO in high wavenumber modes decays faster with redshift as expected.

2.3 BAO in the bispectrum

We define the BAO feature in the bispectrum similarly to that of the power spectrum. We measure the angularly averaged bispectrum - $B(k_1, k_2, k_3)$ - from *withBAO* and *noBAO* GLAM simulations, B_w and B_s respectively (see Appendix A for the details). We bin each wavevector in 30 bins similar to how we did it for the power spectrum. This results in a total of 2600 bins for the (k_1, k_2, k_3) triplet. To map the 3D configuration space of triangles into a 1D index for analysis, we employ a “triangle index” that orders the triangles so that $k_1 \leq k_2 \leq k_3$. This ensures each unique triplet is only counted

¹ <https://www.skiesanduniverses.org/Products/MockCatalogues/GLAMDESILRG/>

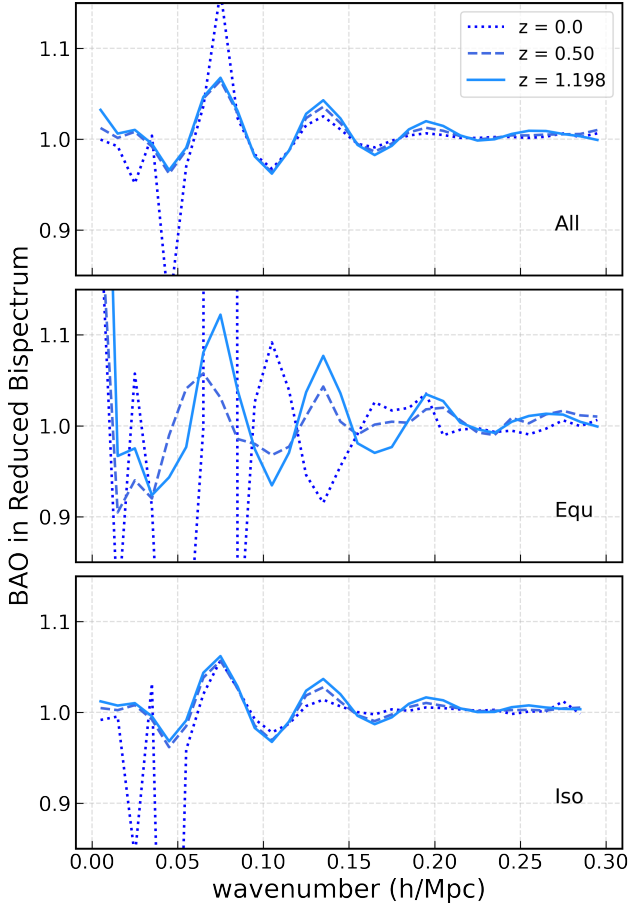


Figure 3. BAO signature in the bispectrum of GLAM simulations at different redshifts. Labels All (top panel), Equ (middle panel), and Iso (lower panel) refer to averages over all, equilateral, and isosceles configurations respectively.

once without duplication since the bispectrum is invariant to any permutation of the indices.

Figure 3 shows the ratio of B_w to B_s at different redshifts. For better visualization, the measurements are averaged over k_2 and k_3 for different triangular configurations. We look at three different averages. In $B^{\text{all}}(k)$ the value of k_1 is kept within a certain bin while all other values of k_2 and k_3 are averaged over. In $B^{\text{iso}}(k)$ we average over bispectra that have the value of k_1 within a certain bin and $k_2 = k_3$. In $B^{\text{equ}}(k)$ we average over all bispectra that have all three wavenumbers within a certain bin.

$$B^{\text{all}}(k) = \sum_{k_2, k_3} \frac{B(k, k_2, k_3)}{N_k} \quad (3)$$

$$B^{\text{iso}}(k) = \sum_{k_2, k_3} \frac{B(k, k_2, k_3)_{k \neq k_2 = k_3}}{N_{k \neq k_2 = k_3}} \quad (4)$$

$$B^{\text{equ}}(k) = \sum_{k_2, k_3} \frac{B(k, k_2, k_3)_{k = k_2 = k_3}}{N_{k = k_2 = k_3}}, \quad (5)$$

where, N_k , $N_{k \neq k_2 = k_3}$ and $N_{k = k_2 = k_3}$ are the number of triangles that fall into the relevant configurations. We only do this to make the comprehension of the plots easier. All our analysis are performed on the original (pre-averaged) 2600 bispectrum measurements.

Even though this averaging is not optimal for the retention of the

BAO feature, it is still clearly visible in all configurations. The equilateral configuration has the most noise since each point in the k axis corresponds only to a single equilateral triangle. In the bispectrum, the BAO feature looks qualitatively similar. It is a decaying oscillation which is more pronounced at higher redshifts.

3 BAO MODELING

3.1 Power spectrum

To model the BAO in the power spectrum we start with the linear model $P_{\text{lin}}(k)$ that we compute using computer code CAMB (Lewis & Bridle 2002) in a fiducial cosmological model. We split this power spectrum into BAO and smooth parts, $P_{\text{lin}}^{\text{BAO}}$ and $P_{\text{lin}}^{\text{s}}$ respectively, using cosmoprime package. cosmoprime has many options for performing this split. We use the option based on the work in Wallisch (2018) and Hamann et al. (2010), but we verified that this choice does not affect our results. We reduce the BAO feature by damping it with a Gaussian term $D(k, \Sigma) = \exp(-\Sigma^2 k^2/2)$ so that our final power spectrum template is

$$P^w(k; \alpha, \Sigma) = P_{\text{lin}}^{\text{s}}(k) [(P_{\text{lin}}^{\text{BAO}}(\alpha k) - 1)D(k, \Sigma) + 1] \quad (6)$$

The dilation parameter α is only applied to the BAO wiggles. The superscript w denotes the fact that the template has BAO wiggles in it. We use just the smooth part of the linear power spectrum as the no-wiggle template.

$$P^{\text{nw}}(k) = P_{\text{lin}}^{\text{s}}(k) \quad (7)$$

Formally, this is a limit $\Sigma \rightarrow 0$ of the wiggle template.

3.2 Bispectrum

Our bispectrum BAO model is inspired by the leading order perturbation theory with linear local bias given by Scoccimarro (2000).

$$B(\mathbf{k}_1, \mathbf{k}_2, \mathbf{k}_3) = 2\mathbf{Z}_1(\mu_1)\mathbf{Z}_1(\mu_2)\mathbf{Z}_2P(\alpha k_1)P(\alpha k_2) + \text{cyclic terms} + [P(k_1) + P(k_2) + P(k_3)]S_1 + S_0, \quad (8)$$

where,

$$\mathbf{Z}_1(\mu) = (b_1 + f\mu_1^2), \quad (9)$$

$$\mathbf{Z}_2 = \left[\frac{b_2}{2} + b_1 F_2(\mathbf{k}_1, \mathbf{k}_2) + f\mu_3^2 G_2(\mathbf{k}_1, \mathbf{k}_2) - \frac{f\mu_3 k_3}{2} \left(\frac{\mu_1}{k_1} (b_1 + f\mu_2^2) + \frac{\mu_2}{k_2} (b_1 + f\mu_1^2) \right) \right], \quad (10)$$

$\mu_i = \mathbf{k}_i \cdot \hat{\mathbf{z}}/k_i$ with $\mathbf{k}_1 + \mathbf{k}_2 + \mathbf{k}_3 = 0$ to account for the triangular condition.

$$F_2(\mathbf{k}_1, \mathbf{k}_2) = \frac{5}{7} + \frac{\mathbf{k}_1 \cdot \mathbf{k}_2}{2k_1 k_2} \left(\frac{k_1}{k_2} + \frac{k_2}{k_1} \right) + \frac{2}{7} \left(\frac{\mathbf{k}_1 \cdot \mathbf{k}_2}{k_1 k_2} \right)^2, \quad (11)$$

and

$$G_2(\mathbf{k}_1, \mathbf{k}_2) = \frac{3}{7} + \frac{\mathbf{k}_1 \cdot \mathbf{k}_2}{2k_1 k_2} \left(\frac{k_1}{k_2} + \frac{k_2}{k_1} \right) + \frac{4}{7} \left(\frac{\mathbf{k}_1 \cdot \mathbf{k}_2}{k_1 k_2} \right)^2, \quad (12)$$

The cyclic terms can be derived by replacing indices 1 and 2 in

the first term with 2 and 3, and 1 and 3 respectively. f , b_1 , b_2 , S_0 and S_1 are free parameters of the fit.

Gagrani & Samushia (2017) showed that most of the information is in the azimuthal averages of the first three even multipoles with $m = 0$ in the multipole expansion containing most of the information relevant to the derivation of cosmological constraints. In this work, we only consider the angularly averaged bispectrum (or the monopole) defined as

$$B_0(k_1, k_2, k_3) = \int_{-1}^{+1} d(\cos \theta_1) \int_0^{2\pi} d\phi B(k_1, k_2, k_3, \theta_1, \phi). \quad (13)$$

We integrate the five-dimensional bispectrum numerically to obtain the three-dimensional bispectrum monopole.

The model depends on wavevector lengths k_1 , k_2 and k_3 , a dilation parameter α and nuisance parameters b_1 , b_2 , and f . In perturbation theory, the last three parameters have a physical meaning (e.g. f is interpreted as a growth rate of structure). We treat these parameters as true nuisance parameters. Their only purpose is to give us a reasonable range of bispectrum shapes to separate the BAO feature. We do not assign to them any physical meaning.

We compute B by using P^w and B^s by using the no-wiggled template P_s . The ratio B/B^s then gives a model for the BAO signature in the bispectrum.

In the end, the model depends on parameters α , b_1 , b_2 , f , S_0 , S_1 , and Σ .

This single universal scaling model is not accurate at the sub-percent precision (Khomeriki & Samushia 2023) but we ignore the higher order effects in this work since they do not really affect any of our main conclusions.

4 BAO FITTING

We fit the model described in section 3 to the GLAM measurements described in section 2 by running a Monte Carlo Markov Chain (MCMC) using the emcee Python package (Foreman-Mackey et al. 2013). The MCMC was run with 70 walkers for 2000 steps, discarding the first 800 steps as burn-in to ensure convergence. The chain is run over α and 6 nuisance parameters (f , b_1 , b_2 , S_0 , S_1 , Σ). The first three parameters in that list control the relative amplitude at different wavenumber triplets, the next two provide wavenumber-dependent and wavenumber-independent additive terms to remove the effect of shot noise, and the last parameter controls how pronounced the BAO feature is. The parameter priors are wide enough to encompass all areas of high likelihood. We find the best-fit values by minimizing

$$\chi^2 = \sum_{ij} X_i W_{ij} X_j, \quad (14)$$

where X is a vector of measurements (either P_w/P_s at different wavenumber or B_w/B_s at different wavenumber triplets) and W_{ij} are weights that upweight or downweight a relative contribution from different wavenumbers to the overall fit. The most optimal weights are the ones given by the inverse covariance of our measurements. Unfortunately, we don't have a reliable way of estimating the inverse covariance. We use the inverse of a sample variance over 1,000 GLAM mocks as our weights. We can not use the posterior of our likelihood to approximate the true constraining power of the BAO signal in the bispectrum since the sample covariance computed from a small number of mocks is a very noisy estimator of a true covariance and the Hartlap correction factor (Hartlap et al. 2007), commonly used to unbiased the inverse of the covariance matrix, was not applied in this

case due to the insufficient number of realizations. The minimum of the Eq. 14 is still an unbiased estimator and we can use it to estimate the systematic offsets in our fits. Our measurements are computed from a very large cumulative volume of $1,000h^{-1}$ Gpc and we expect the uncertainty in the systematic offset to be negligible.

α is the only parameter of interest to us, the other six are nuisance parameters that we marginalize over. We have another hidden degree of freedom in this fit, which is the fiducial cosmology that we choose to produce the original P_{lin} template. We are hoping that no matter which template we start with, it can be made to fit the measurements by an appropriate rescaling of the oscillation frequency with α and damping the amplitude of oscillations at high wavenumbers with Σ . The dilation parameter is expected to be

$$\alpha = \frac{r_{\text{d}}^{\text{tmp}}}{r_{\text{d}}}. \quad (15)$$

We do not have scaling with D_V like in Eq. (1). This is because we are measuring our bispectra in cubic boxes with known physical size and we are not affected by Alcock-Paczynski scaling. We will show the results of fitting to the redshift $z = 0.5$, but we also verified that the same conclusions hold for redshifts $z = 0$ and $z = 1.198$.

4.1 Aligned Template

We first check what happens when the template is computed in the actual cosmology of GLAM simulations. In this case, the BAOs in the template and the measurements are aligned and the expected value of α is one. The results from running our MCMC chains for the aligned template for the redshift of $z = 0.5$ are shown in Figure 4. The results for other redshifts look qualitatively similar. The likelihood contours are reasonably close to Gaussian. While some of the nuisance parameters are correlated with each other, the α_V parameter is uncorrelated with any of the nuisance parameters, suggesting that its maximum likelihood values are weakly affected by possible posterior volume effects. The f parameter is allowed to take on negative values, under the standard interpretation of its meaning this would be unphysical. We, however, do not interpret f as a growth rate of structure but rather use it as a pure nuisance parameter that is used to help us span the range of possible shapes for the smooth part of the bispectrum, so this is not a problem for our analysis. We checked that restricting f to have only positive values does not affect constraints on α , which is not surprising since f and α are very weakly correlated. Our recovered value of α is consistent with unity to 0.03 percent precision. It's worth noting that since we do not have reliable estimates of the covariance matrix, the widths of our MCMC chains can not be interpreted as errors in the measurement. We do not have at present a good way of estimating the variance in our measurements but we expect it to be subdominant to the systematic error from the fit since we are fitting the mean measurement of 1,000 one cubic Gigaparsec mocks.

Figure 5 shows the bispectrum BAOs from GLAM measurements at redshifts 0.0, 0.5, and 1.198, and their corresponding best-fit models evaluated at the best values derived from MCMC chains. The models match the measurements well and by visual inspection successfully recover all features in the measurements. Figure 6 shows the same information but now as a ratio of the predicted and measured bispectra. At $z = 0.0$ there are some bispectrum triplets that have a large fractional deviation between the measurement and the theory. This is likely the failure of the simple model adopted in our work which does capture the overall frequency of the BAO oscillations well but fails to predict the amplitude of the BAO for some triplets.

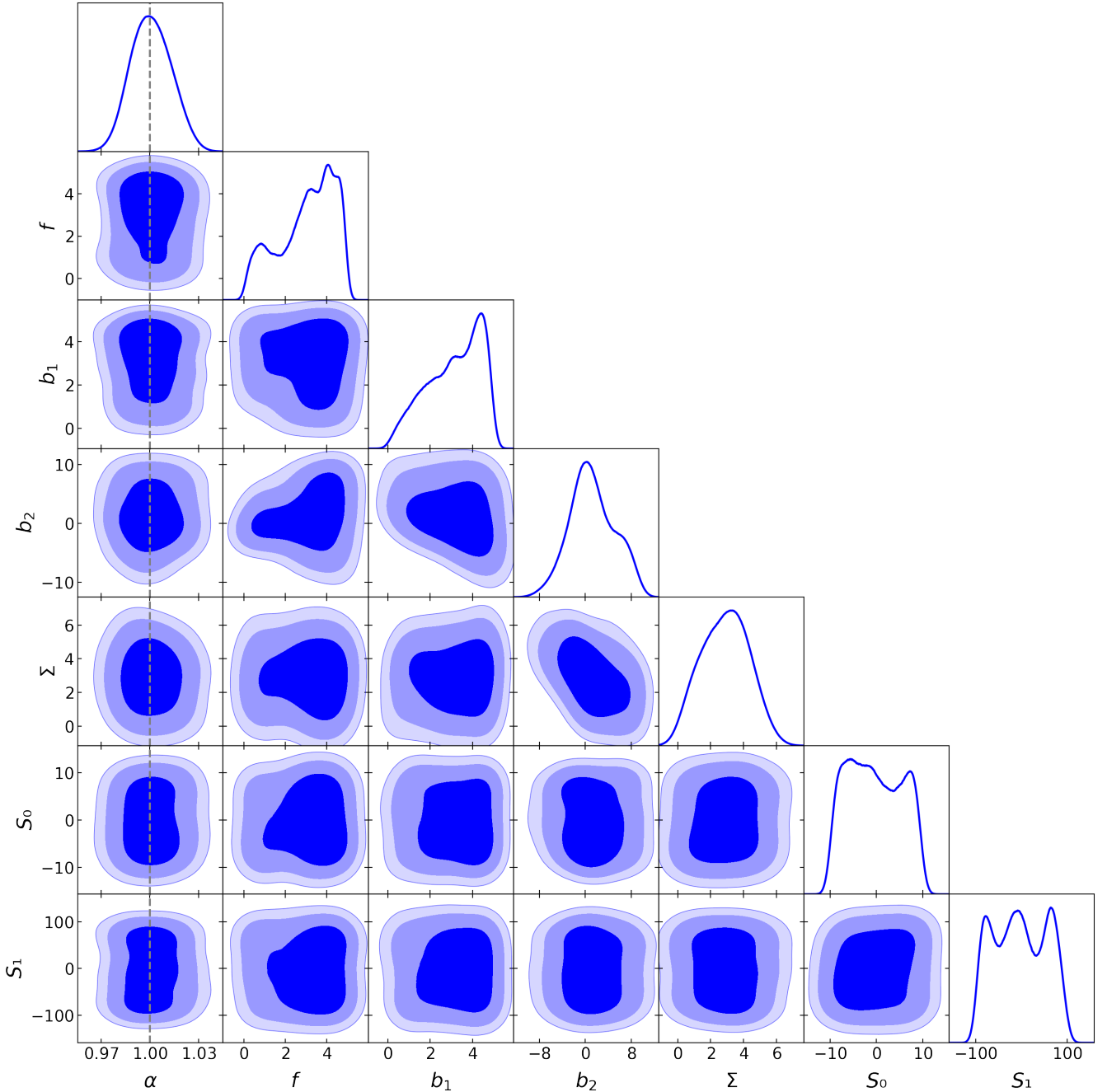


Figure 4. Equipotential contours of the MCMC posterior from fitting the BAO in GLAM bispectrum at $z = 0.5$. The grey dashed line shows the expected value of $\alpha = 1$.

Figure 7 shows a similar best fit to the entire bispectrum (not the BAO only like in the previous case). As expected the simple model can not fit the full shape of the bispectrum well, there are obvious and irreconcilable offsets between the measured and theoretical bispectra at a wide range of wavenumbers and triangular configurations.

To aid visual inspection we also plot the measured and best-fit model bispectra for averaged, isosceles, and equilateral triangles as defined by Eqs. (3)–(5). Figure 8 shows this comparison for the bispectrum measured at $z = 0.5$. The top panel shows the GLAM BAOs along with the model computed for the original templates derived

from CAMB. The middle row shows the effect of the damping parameter Σ on the model for the best-fit Σ from the MCMC chains. The bottom row shows the result of stretching it by the best-fit value of α . Since our best-fit is very close to one, the best-fit BAO template is difficult to distinguish from the “true” BAO template (evaluated at $\alpha_{\text{V}} = 1$), which we also plot on the same figures for comparison. Visual inspection confirms that the best-fit template is indeed a good fit for the harmonic feature imprinted in the measurements. The template seems to be offset for the equilateral triangles. This can be explained by high noise in this specific measurement. The averaged

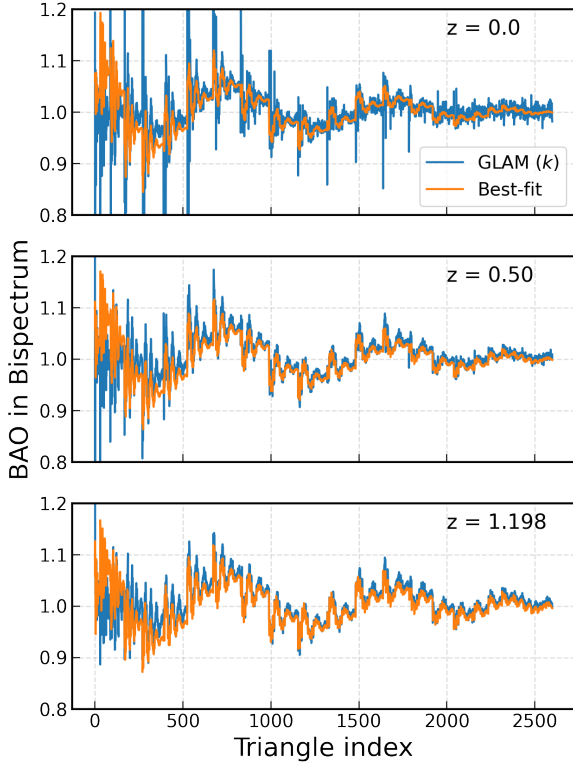


Figure 5. BAO signature in the bispectrum as a function of triangle index (see definition in Sec 2.3) at different redshifts. Measured bispectrum BAOs from the GLAM simulations (the blue line) is compared to our best-fit model (the orange line).

and isosceles measurements are averages over many triangular configurations, while the equilateral measurement is averaged over very few triangular configurations.

4.2 Systematic effects due to offset template

We now check whether the model performs equally well when the template is computed in a different cosmology from the GLAM so that the position of the BAO peak is offset. To perform this test we generate templates in 100 different cosmologies around GLAM cosmology in a range $0.277 \leq \Omega_m \leq 0.327$. We then perform the fitting as before. Figure 9 shows the results of this exercise. Each point on the top panel corresponds to a template used in the fits. The horizontal axis shows the expected value of α and the vertical axis shows the percentage offset of the best fit from that expectation. In the ideal case, we want the points to be as close as possible to zero. The bottom panel shows the same data from a different point of view. The points are again individual templates, the horizontal axis is the value of r_d in the template and α is the amount of dilation needed to bring the template to be identical to the true BAO signal. Blue dots show our expectations and the orange dots show the actual results. We expected the systematic offset between the two to increase as the offset between the template and the simulations increases, which

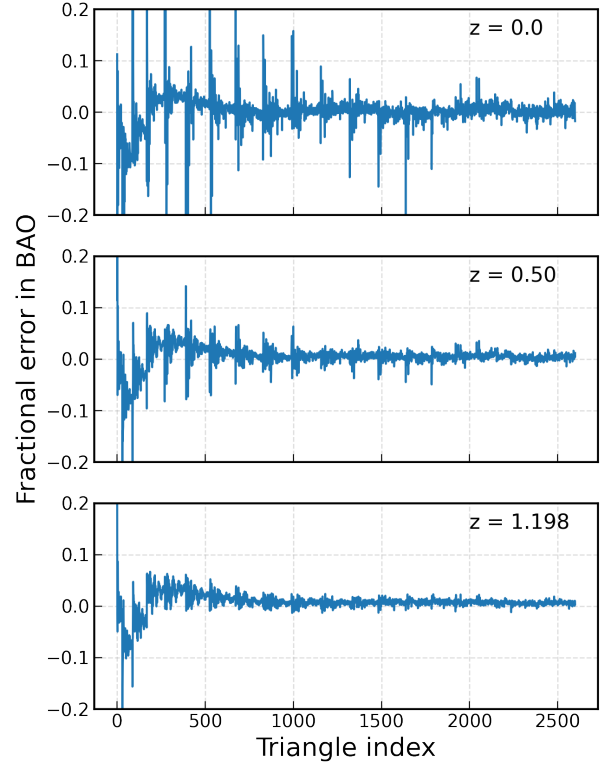


Figure 6. Fractional deviation between the measured bispectrum BAOs from the GLAM simulations and our best-fit model as a function of triangle index (see definition in Sec 2.3) at different redshifts.

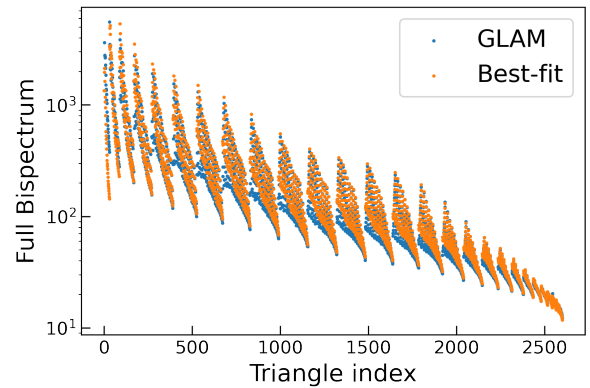


Figure 7. Full bispectrum as a function of triangle index (see definition in Sec 2.3) at redshift 0.5. Measured bispectrum from the GLAM simulations (the blue line) is compared to our best-fit model (the orange line).

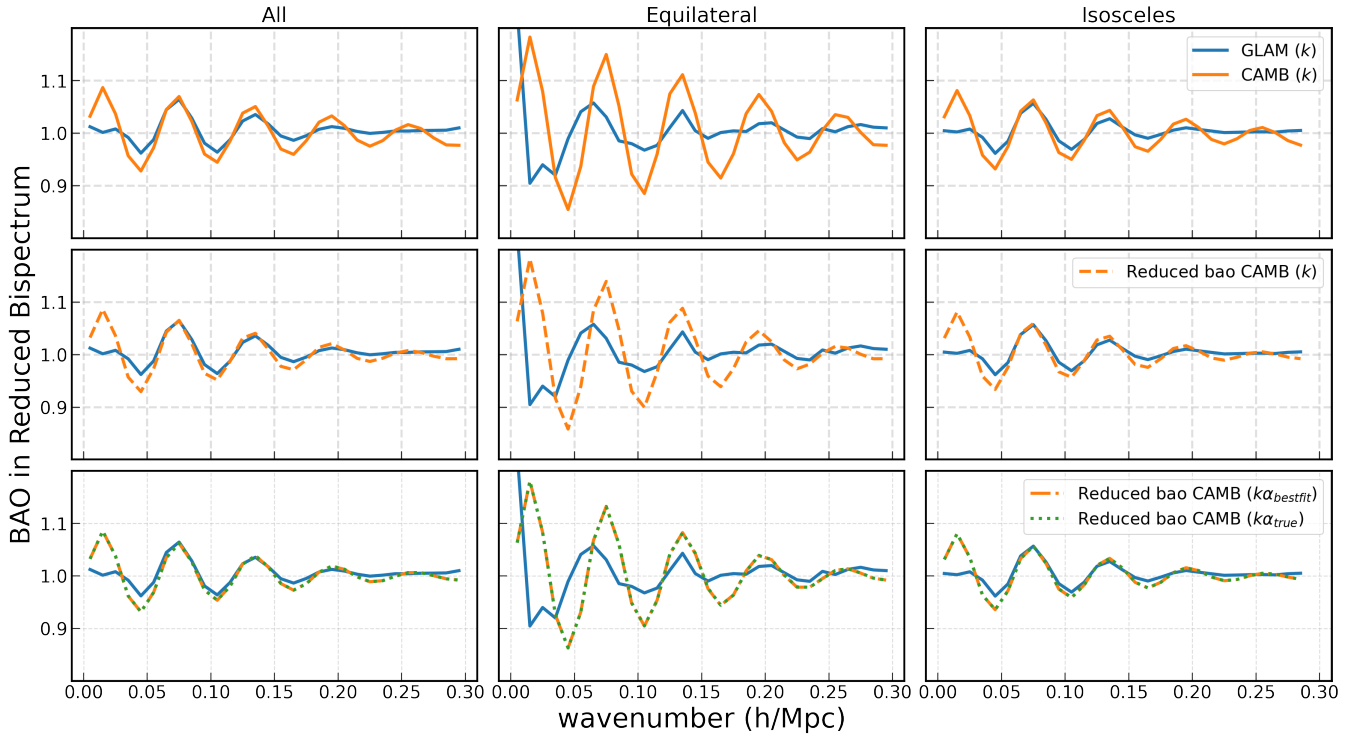


Figure 8. Measured BAO in the bispectrum compared to the model. The columns show bispectrum averaged over all (left), equilateral (middle), and isosceles (right) configurations. The blue lines denote the measurements and are identical along the columns. The solid orange lines in the top row denote the model computed based on a CAMB linear power spectrum. The dashed orange lines in the middle row denote the model with the BAO damping applied, which reduces the amplitude of the BAO wiggles. The dot-dashed yellow line and the dotted green line in the bottom row denote the model stretched by the best fit and true α values respectively.

seems to be the case. The systematic offsets are mostly within 0.3 per cent as long as the frequency of the BAO in the template does not differ by more than 3 per cent from the frequency in the data.

5 CONCLUSIONS

We explored the possibility of modeling the BAO feature in the galaxy bispectrum. Even though some of this information is recovered during the reconstruction of the cosmological fields, the measurements of the BAO in the galaxy bispectrum have the potential to strengthen our constraints on key cosmological parameters. In the measured bispectrum the BAO signal is visible at wavenumber as high as $k \sim 0.3h^{-1}$ Mpc at redshifts of $z = 0.5$ and above. At lower redshifts, the BAO signature at higher wavenumber is damped by nonlinear evolution. We showed that even though simple perturbation-based models of bispectrum fail to model it accurately at higher wavenumbers, they work reasonably well when the smooth component is subtracted and only the BAO feature is modeled. We validated this on a suit of GLAM simulations that have been run with and without the BAO feature in the initial conditions. The ratio of the bispectra measured from those simulations is by definition the BAO feature in the bispectrum. Our six-parameter model was able to recover the unbiased value of α parameter when fit to the bispectrum monopole measured from a cumulative volume of $1,000 h^{-3} \text{Gpc}^3$. In real analysis, we don't know a priori what cosmological model to use when producing BAO templates. It is therefore important that the procedure results in unbiased results for a range of reasonable templates. We checked the

robustness of the model by fitting the same measurements with the templates computed in offset cosmologies. By performing similar validation tests we demonstrated that the bias in the recovered values of α is at most 0.3 per cent for deviations up to 3 per cent from the true value of the sound horizon. This is good enough when fitting to currently existing data but may need improvement when future more precise data arrives (e.g. from the DESI and Euclid experiments). Possible avenues for decreasing the bias are computing the BAO template with more sophisticated modeling of nonlinear physics or using simulations for calibrating the templates.

ACKNOWLEDGEMENTS

We are grateful to Francisco Prada and Anatoly Klypin for their help with GLAM simulations.

This research used resources of the National Energy Research Scientific Computing Center (NERSC), a U.S. Department of Energy Office of Science User Facility located at Lawrence Berkeley National Laboratory, operated under Contract No. DE-AC02-05CH11231

This research has made use of NASA's Astrophysics Data System and the arXiv open-access repository of electronic preprints and postprints.

JB, MR, and LS are grateful for support from the US Department of Energy via grants DE-SC0021165 and DE-SC0011840. JB is partially supported by the NASA ROSES grant 12-EUCLID12-0004. JE acknowledges financial support from the Spanish MICINN funding

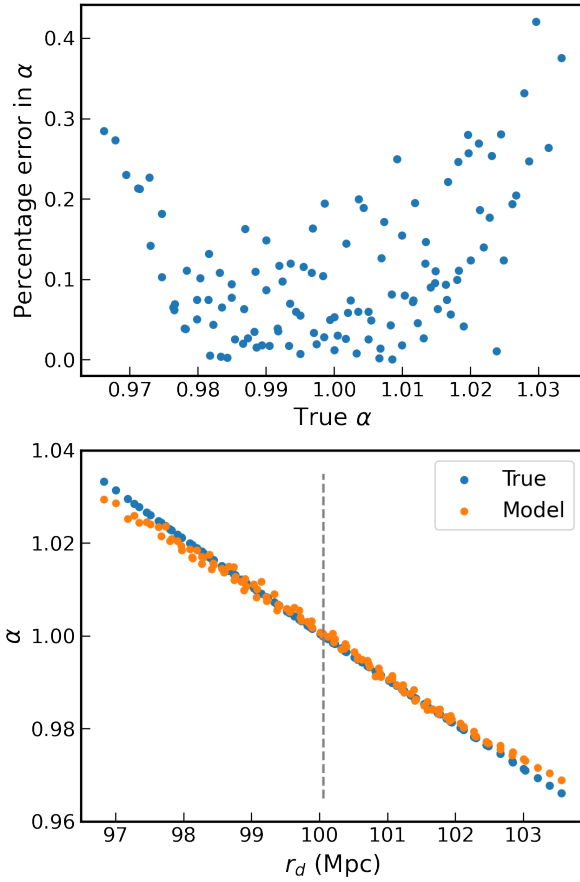


Figure 9. Percentage systematic error in the recovered value of α as a function of the expected alpha.

grant PGC2018-101931-B-I00. We thank Instituto de Astrofísica de Andalucía CSIC for hosting the Skies & Universes site for cosmological simulation products. GLAM A-series simulations were performed at the DIRAC@Durham facility managed by the Institute for Computational Cosmology on behalf of the STFC DiRAC HPC Facility in the UK.

DATA AVAILABILITY

Any data product generated during this research will be shared upon request. The GLAM simulations are available for download from <https://www.skiesanduniverses.org/Products/MockCatalogues/GLAMDESILRG/>.

REFERENCES

Abbott T. M. C., et al., 2018, *Phys. Rev. D*, **98**, 043526
 Alam S., et al., 2017, *MNRAS*, **470**, 2617

- Alesta G., Kazantzidis L., Perivolaropoulos L., 2020, *Phys. Rev. D*, **101**, 123516
 Alkhanishvili D., Porciani C., Sefusatti E., Biagetti M., Lazanu A., Oddo A., Yankelevich V., 2022, *MNRAS*, **512**, 4961
 Anderson L., et al., 2012, *MNRAS*, **427**, 3435
 Anderson L., et al., 2014, *MNRAS*, **441**, 24
 Ata M., et al., 2018, *MNRAS*, **473**, 4773
 Aubourg É., et al., 2015, *Phys. Rev. D*, **92**, 123516
 Babić I., Schmidt F., Tucci B., 2022, *J. Cosmology Astropart. Phys.*, **2022**, 007
 Baldauf T., Mirbabayi M., Simonović M., Zaldarriaga M., 2015, *Phys. Rev. D*, **92**, 043514
 Baldauf T., Garny M., Taule P., Steele T., 2021, *Phys. Rev. D*, **104**, 123551
 Baugh C. M., et al., 2019, *MNRAS*, **483**, 4922
 Bautista J. E., et al., 2021, *MNRAS*, **500**, 736
 Betoule M., et al., 2014, *A&A*, **568**, A22
 Beutler F., et al., 2017a, *MNRAS*, **464**, 3409
 Beutler F., et al., 2017b, *MNRAS*, **466**, 2242
 Blazek J., Seljak U., Vlah Z., Okumura T., 2014, *J. Cosmology Astropart. Phys.*, **2014**, 001
 Bond J. R., Efstathiou G., 1984, *ApJ*, **285**, L45
 Bond J. R., Efstathiou G., 1987, *MNRAS*, **226**, 655
 Bose B., Taruya A., 2018, *J. Cosmology Astropart. Phys.*, **2018**, 019
 Brigham E. O., 1988, *The fast Fourier transform and its applications*.
 Byun J., Agarwal N., Bean R., Holman R., 2015, *Phys. Rev. D*, **91**, 123518
 Byun J., Eggemeier A., Regan D., Seery D., Smith R. E., 2017, *MNRAS*, **471**, 1581
 Chen S.-F., Vlah Z., White M., 2019, *J. Cosmology Astropart. Phys.*, **2019**, 017
 Colavincenzo M., et al., 2019, *MNRAS*, **482**, 4883
 Crocce M., Scoccimarro R., Bernardreau F., 2012, *MNRAS*, **427**, 2537
 Cuesta A. J., et al., 2016, *MNRAS*, **457**, 1770
 Di Valentino E., Melchiorri A., Mena O., Vagnozzi S., 2020, *Phys. Rev. D*, **101**, 063502
 Ding Z., Seo H.-J., Vlah Z., Feng Y., Schmittfull M., Beutler F., 2018, *MNRAS*, **479**, 1021
 Eisenstein D. J., Seo H.-J., White M., 2007, *ApJ*, **664**, 660
 Escamilla L. A., Giarè W., Di Valentino E., Nunes R. C., Vagnozzi S., 2023, *arXiv e-prints*, p. [arXiv:2307.14802](https://arxiv.org/abs/2307.14802)
 Fonseca de la Bella L., Regan D., Seery D., Hotchkiss S., 2017, *J. Cosmology Astropart. Phys.*, **2017**, 039
 Foreman-Mackey D., Hogg D. W., Lang D., Goodman J., 2013, *PASP*, **125**, 306
 Gagrani P., Samushia L., 2017, *MNRAS*, **467**, 928
 Geçkinli N. C., Yavuz D., 1983, *Discrete Fourier transformation and its applications to power spectra estimation*
 Gil-Marín H., et al., 2016, *MNRAS*, **460**, 4210
 Gil-Marín H., Percival W. J., Verde L., Brownstein J. R., Chuang C.-H., Kitaura F.-S., Rodríguez-Torres S. A., Olmstead M. D., 2017, *MNRAS*, **465**, 1757
 Gil-Marín H., et al., 2018, *MNRAS*, **477**, 1604
 Gil-Marín H., et al., 2020, *MNRAS*, **498**, 2492
 Grieb J. N., et al., 2017, *MNRAS*, **467**, 2085
 Gualdi D., Gil-Marín H., Manera M., Joachimi B., Lahav O., 2019, *MNRAS*, **484**, L29
 Guidi M., Veropalumbo A., Branchini E., Eggemeier A., Carbone C., 2023, *J. Cosmology Astropart. Phys.*, **2023**, 066
 Hamann J., Hannestad S., Lesgourgues J., Rampf C., Wong Y. Y. Y., 2010, *J. Cosmology Astropart. Phys.*, **2010**, 022
 Hartlap J., Simon P., Schneider P., 2007, *A&A*, **464**, 399
 Hernández-Aguayo C., Prada F., Baugh C. M., Klypin A., 2021, *Monthly Notices of the Royal Astronomical Society*, **503**, 2318
 Hinton S. R., Howlett C., Davis T. M., 2020, *MNRAS*, **493**, 4078
 Hoffmann K., Gaztañaga E., Scoccimarro R., Crocce M., 2018, *MNRAS*, **476**, 814
 Holtzman J. A., 1989, *ApJS*, **71**, 1
 Hou J., et al., 2018, *MNRAS*, **480**, 2521
 Hou J., et al., 2021, *MNRAS*, **500**, 1201

Ivanov M. M., Simonović M., Zaldarriaga M., 2020, *J. Cosmology Astropart. Phys.*, 2020, 042

Ivanov M. M., Philcox O. H. E., Nishimichi T., Simonović M., Takada M., Zaldarriaga M., 2022, *Phys. Rev. D*, 105, 063512

Karandikar M., Porciani C., Hahn O., 2023, *arXiv e-prints*, p. arXiv:2307.11090

Khomeriki G., Samushia L., 2023, *arXiv e-prints*, p. arXiv:2307.16498

Klypin A., Prada F., 2018, *MNRAS*, 478, 4602

Lazanu A., Giannantonio T., Schmittfull M., Shellard E. P. S., 2016, *Phys. Rev. D*, 93, 083517

Lewis A., Bridle S., 2002, *Phys. Rev. D*, 66, 103511

Meiksin A., White M., Peacock J. A., 1999, *MNRAS*, 304, 851

Neveux R., et al., 2020, *MNRAS*, 499, 210

Noh Y., White M., Padmanabhan N., 2009, *Phys. Rev. D*, 80, 123501

Nomura H., Yamamoto K., Nishimichi T., 2008, *J. Cosmology Astropart. Phys.*, 2008, 031

Oddo A., Sefusatti E., Porciani C., Monaco P., Sánchez A. G., 2020, *J. Cosmology Astropart. Phys.*, 2020, 056

Padmanabhan N., White M., 2008, *Phys. Rev. D*, 77, 123540

Pearson D. W., Samushia L., 2018, *MNRAS*, 478, 4500

Peebles P. J. E., Yu J. T., 1970, *ApJ*, 162, 815

Philcox O. H. E., Ivanov M. M., 2022, *Phys. Rev. D*, 105, 043517

Philcox O. H. E., Ivanov M. M., Cabass G., Simonović M., Zaldarriaga M., Nishimichi T., 2022, *Phys. Rev. D*, 106, 043530

Planck Collaboration et al., 2014, *A&A*, 571, A16

Planck Collaboration et al., 2020, *A&A*, 641, A6

Prada F., Scóccola C. G., Chuang C.-H., Yepes G., Klypin A. A., Kitaura F.-S., Gottlöber S., Zhao C., 2016, *MNRAS*, 458, 613

Raichoor A., et al., 2021, *MNRAS*, 500, 3254

Ramirez R. W., 1985, *The FFT. Fundamentals and concepts*

Reid B. A., et al., 2012, *MNRAS*, 426, 2719

Rizzo F., Moretti C., Pardede K., Eggeimer A., Oddo A., Sefusatti E., Porciani C., Monaco P., 2023, *J. Cosmology Astropart. Phys.*, 2023, 031

Ross A. J., Percival W. J., Manera M., 2015, *MNRAS*, 451, 1331

Ross A. J., et al., 2017, *MNRAS*, 464, 1168

Samushia L., Slepian Z., Villaescusa-Navarro F., 2021, *MNRAS*, 505, 628

Sánchez A. G., et al., 2017, *MNRAS*, 464, 1640

Scoccimarro R., 2000, *ApJ*, 544, 597

Sefusatti E., Crocce M., Scoccimarro R., Couchman H. M. P., 2016, *MNRAS*, 460, 3624

Seo H.-J., Eisenstein D. J., 2005, *ApJ*, 633, 575

Seo H.-J., Beutler F., Ross A. J., Saito S., 2016, *MNRAS*, 460, 2453

Silk J., 1968, *ApJ*, 151, 459

Slepian Z., Eisenstein D. J., 2015, *MNRAS*, 454, 4142

Slepian Z., et al., 2017, *MNRAS*, 468, 1070

Springel V., et al., 2005, *Nature*, 435, 629

Sugiyama N. S., Saito S., Beutler F., Seo H.-J., 2019, *MNRAS*, 484, 364

Sugiyama N. S., Saito S., Beutler F., Seo H.-J., 2020, *MNRAS*, 497, 1684

Sugiyama N. S., Saito S., Beutler F., Seo H.-J., 2021, *MNRAS*, 501, 2862

Sugiyama N. S., et al., 2023a, *MNRAS*, 523, 3133

Sugiyama N. S., et al., 2023b, *MNRAS*, 524, 1651

Sunyaev R. A., Zeldovich Y. B., 1970, *Ap&SS*, 7, 3

Thepsuriya K., Lewis A., 2015, *J. Cosmology Astropart. Phys.*, 2015, 034

Tröster T., et al., 2020, *A&A*, 633, L10

Valageas P., Nishimichi T., 2020, *Phys. Rev. D*, 102, 043530

Vargas Magaña M., et al., 2013, *arXiv e-prints*, p. arXiv:1312.4996

Vargas-Magaña M., et al., 2014, *MNRAS*, 445, 2

Vlah Z., White M., Aviles A., 2015, *J. Cosmology Astropart. Phys.*, 2015, 014

Wallisch B., 2018, PhD thesis, University of Cambridge, UK

White M., 2005, *Astroparticle Physics*, 24, 334

Zhu F., et al., 2018, *MNRAS*, 480, 1096

d'Amico G., Gleyzes J., Kokron N., Markovic K., Senatore L., Zhang P., Beutler F., Gil-Marín H., 2020, *J. Cosmology Astropart. Phys.*, 2020, 005

de Mattia A., et al., 2021, *MNRAS*, 501, 5616

APPENDIX A: MEASURING POWER SPECTRUM AND BISPECTRUM

We divide every simulation cube into a 1024^3 grid. We assign halos to grid points based on the triangular shaped cloud scheme described in (Sefusatti et al. 2016) to compute the number of particles in each grid cell - n_{ijk} . We then compute the overdensity field

$$\delta_{ijk} = \frac{n_{ijk} - \bar{n}}{\bar{n}}, \quad (\text{A1})$$

where \bar{n} is the average number density

$$\bar{n} = \frac{1}{1024^3} \sum_{ijk} n_{ijk}. \quad (\text{A2})$$

We then perform a 3D discrete Fourier transform of the overdensity field

$$\tilde{\delta}_{ijk} = \mathcal{F}_{ijk}^{\ell mn} [\delta_{\ell mn}]. \quad (\text{A3})$$

The $\tilde{\delta}_{ijk}$ numbers can be arranged in a 3D cube so that each measurement corresponds to a certain wavevector $\mathbf{k} = (k_i, k_j, k_k)$ (Geçkinli & Yavuz 1983; Ramirez 1985; Brigham 1988). The average power spectrum within a bin (k_{\min}, k_{\max}) is computed as the average value of all $\tilde{\delta}_{ijk} \tilde{\delta}_{ijk}^*$ such that the length $|\mathbf{k}| = \sqrt{k_i^2 + k_j^2 + k_k^2}$ falls within the bin. The average bispectrum within a bin $(k_{i,\min}, k_{i,\max})$, where $i = (1, 2, 3)$ is similarly computed as the average of all $\tilde{\delta}_{i_1 j_1 k_1} \tilde{\delta}_{i_2 j_2 k_2} \tilde{\delta}_{i_3 j_3 k_3}$ such that wavevectors associated to the three $\tilde{\delta}$ fall within the corresponding bins and their sum is zero.

This paper has been typeset from a \LaTeX file prepared by the author.